ACS APPLIED MATERIALS & INTERFACES

Research Article

www.acsami.org

Enhancing the Spin–Orbit Coupling in Fe_3O_4 Epitaxial Thin Films by Interface Engineering

Zhaocong Huang,[*,†,‡,∥] Wenqing Liu,[‡,⊥] Jinjin Yue,[†] Qionghua Zhou,[†] Wen Zhang,[†] Yongxiong Lu,[‡] Yunxia Sui,[§] Ya Zhai,[*,†,§] Qian Chen,[†] Shuai Dong,[†] Jinlan Wang,[†] Yongbing Xu,[‡] and Baoping Wang[∥]

[†]Department of Physics, Jiangsu Key Laboratory for Advanced Metallic Materials, Southeast University, Nanjing 211189, China

[‡]Spintronics and Nanodevice Laboratory, Department of Electronics, University of York, York, U.K.

[⊥]Department of Electronic Engineering, Royal Holloway, University of London, Surrey, U.K.

[§]National Laboratory of Solid Microstructures and Center of Modern Analysis, Nanjing University, Nanjing, China

[∥]School of Electronic Science and Engineering, Southeast University, Nanjing 210096, China

Supporting Information

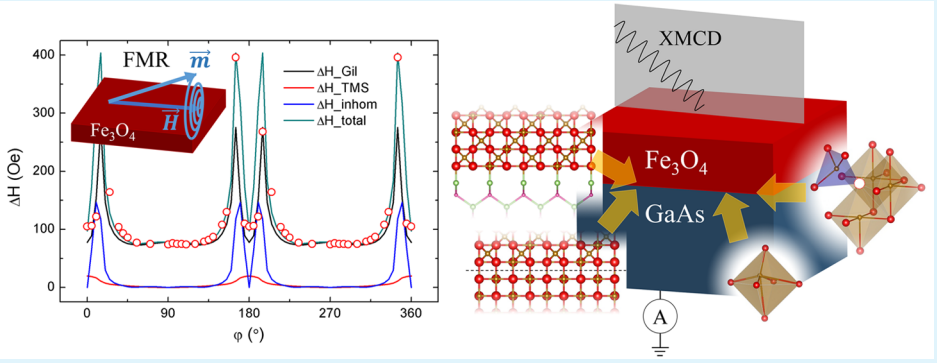

ABSTRACT: By analyzing the in-plane angular dependence of ferromagnetic resonance linewidth, we show that the Gilbert damping constant in ultrathin Fe_3O_4 epitaxial films on GaAs substrate can be enhanced by thickness reduction and oxygen vacancies in the interface. At the same time, the uniaxial magnetic anisotropy due to the interface effect becomes significant. Using the element-specific technique of X-ray magnetic circular dichroism, we find that the orbital-to-spin moment ratio increases with decreasing film thickness, in full agreement with the increase in the Gilbert damping obtained for these ultrathin single-crystal films. Combined with the first-principle calculations, the results suggest that the bonding with Fe and Ga or As ions and the ionic distortion near the interface, as well as the FeO defects and oxygen vacancies, may increase the spin–orbit coupling in ultrathin Fe_3O_4 epitaxial films and in turn provide an enhanced damping.

KEYWORDS: *half metallic Fe_3O_4, spin–orbit coupling, thin film, ferromagnetic resonance, Gilbert damping*

INTRODUCTION

The rapid development of spintronics, in particular, spin–orbitronics, has been strongly linked with the realization of the role of spin–orbit coupling (SOC) in novel physical phenomena like spin Hall effect,[1] spin dynamic damping,[2] topological insulators,[3] and the vortex spin configuration in skyrmion.[4] Large SOC can be used to transform a spin-polarized current to a charge current or vice versa, enabling manipulation of nanoscale spin devices in nonmagnetic materials. It has been recently reported that the strongly spin–orbit coupled topological insulator with magnetic perturbation by using impurities,[5,6] adatoms,[7] or substrate[8,9] leads to enhanced magnetism and the accompanying fascinating quantum effects[10−13] and even produces the half-metal properties.[14,15] For similar reasons in high-spin state systems, for example, ferromagnetic or half-metallic materials, it is possible that large SOC may introduce topological properties. Xiao et al.[16] reported that half-Heusler compounds can be tuned into a new class of three-dimensional topological insulators. Half-metallic Fe_3O_4 is a competitive contender in the race to become one of the key materials in future spintronics computing, or spin-operation-based data processing and sensing, due to its high-spin polarization near the Fermi level (E_F), high Curie temperature (T_c), and good electronic conductivity at room temperature.[17−19] Unquenched m_{orb}, or strong SOC, is a desired property in terms of the controllability by electric field in spintronics operation, however, which has been reported with controversy in magnetite.[20−22] Surfaces and interfaces lack structural inversion symmetry, allowing interfacial SOC to play an expanded role, which generates various

Received: July 30, 2016
Accepted: September 23, 2016
Published: September 23, 2016

DOI: 10.1021/acsami.6b09478
ACS Appl. Mater. Interfaces 2016, 8, 27353−27359

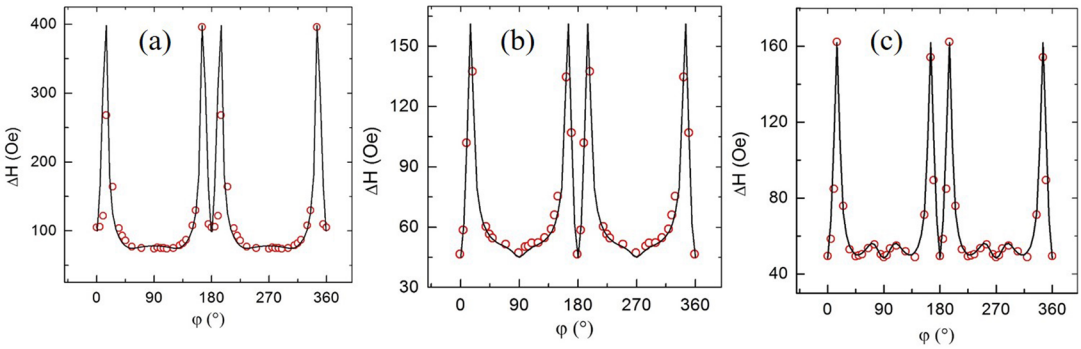

Figure 1. Angular dependence of linewidth ΔH on in-plane orientation φ_H with respect to GaAs(100)[011] direction with different thickness t_{Fe} = (a) 4, (b) 6, and (c) 8 nm. The red circles are the experimental data points, and the solid lines represent the theoretical fitting curves.

effects including the Dzyaloshinskii–Moriya (DM) interaction[23−25] and the spin–orbit torque.[26−28] In this paper, focusing on the enhancement of SOC of ultrathin epitaxial Fe_3O_4 film, by decreasing the film thickness, we investigate the influence of the surface and interface effect.

EXPERIMENTAL AND THEORETICAL METHODS

Fe_3O_4 Film Deposition. Fe_3O_4 ultrathin films with thickness varying from 4 to 8 nm were epitaxially grown on GaAs(001) substrates by molecular beam epitaxy (MBE) using postgrowth oxidation method as illustrated in Supporting Information Figure S1. It has been shown that the magnetic dead layer and the antiphase boundaries could be avoided by the postgrowth oxidation method.[29] First, the substrates were chemically cleaned using an $H_2SO_4/H_2O_2/H_2O$ (4:1:1) solution for 30 s, followed by deionized water rinsing and isopropyl alcohol vapor cleaning. After being transferred into the ultrahigh vacuum chamber, the substrates were annealed at 830 K for ∼30 min until a sharp pattern of reflection high-energy electron diffraction (RHEED) was identified as shown in Supporting Information Figure S2. After Fe films with thicknesses of 4, 6, and 8 nm were grown on the GaAs substrates in MBE chamber, the films were finally oxidized in situ to Fe_3O_4 in an oxygen atmosphere with the O_2 partial pressure of 5×10^{-5} mbar at 500 K. After oxidation for 20 min, no further change of RHEED patterns was observed with further annealing after that. By Fe_3O_4 lattice rotating 45° to match GaAs lattice, the lattice mismatch between Fe_3O_4 and GaAs is ∼5%, and the epitaxial relationships for all samples are all $Fe_3O_4(100)[011]//GaAs(100)[001]$ as suggested by the RHEED.[29] Thereafter, the nominal thicknesses of the predeposited Fe layers (t_{Fe}) will be quoted for the samples after the oxidation.

Material Characterization. The saturation magnetic moments of the Fe_3O_4/GaAs epitaxial films were measured by vibrating sample magnetometer. Ferromagnetic resonance (FMR) measurements were performed with a Bruker ESR equipment of model ER-200D-SRC at a microwave frequency of 9.78 GHz at room temperature. The X-ray magnetic circular dichroism (XMCD) measurements at the Fe $L_{2,3}$ absorption edges were performed at the U.K. National Synchrotron Radiation Laboratory (U.K).

Theoretical Calculation. The ab initio calculations were performed via density functional theory by using a 56-atoms unit cell of $Fe_{24}O_{32}$ model with inverse spinel structure (see Supporting Information Figure S3) with periodic boundary condition. We adopted a projected augmented wave[30] pseudopotential to describe the core electrons and the general gradient approximation of Perdew, Burke, and Ernzerhof[31] for exchange and correlation as implemented by the Vienna Ab-initio Simulation Package).[32] The kinetic energy cutoff was set to 400 eV, and the Brillouin zone was sampled by 5 × 5 × 5 and 7 × 7 × 7 k-point meshes using the Monkhorst–Pack method[33] for geometry optimizations and further calculations on electronic structure and other properties, respectively. All structures were fully relaxed without any symmetry constraint until both the Hellmann–Feynman forces acting on each ion and total energy change are less than 0.005 eV/Å and 1×10^{-4} eV, respectively. The SOC was included in the calculation as a perturbation using the scalar-relativistic eigenfunctions of the valence states.

RESULTS AND DISCUSSION

The saturation magnetic moments (M_s) per formula unit (f.u.) of the Fe_3O_4/GaAs films are shown in the inset of Supporting Information Figure S4a. The M_s of the films with t_{Fe} = 4 and 6 nm are very close to the bulk value of 4 μ_B/f.u., indicating that the films with t_{Fe} = 4 and 6 nm are well-oxidized and as well have the bulk structure in general. However, a great increment of saturation moment in the film with t_{Fe} = 8 nm was found. Because of the postgrowth oxidation process of sample fabrication, considerable oxygen vacancies or non-stoichiometry may appear near the interface of Fe_3O_4 and GaAs in thicker film. Oxygen vacancies, which could be controlled by the fabrication condition, that is, partial oxygen pressure, annealing time, and annealing temperature, are possible to lead the spin of A site Fe ions near the vacancies to switch parallel to the B site Fe ions and in turn enhance the saturation moment.[34]

FMR is one of the most powerful experimental techniques for studying magnetic properties of thin films and can provide sufficient information describing the magnetic properties of thin films, such as magnetic anisotropy and relaxation mechanisms of the magnetization.[35,36] Only one sharp peak for each FMR spectrum is in our films presences, as shown in Supporting Information Figure S4a, indicating that there is only one main magnetic phase of Fe_3O_4 that existed in our samples, which is also suggested by our X-ray photoelectron spectroscopy results.[29,37]

The information on magnetization relaxation damping that is related to the SOC can be obtained from the resonance field and linewidth of FMR spectra. As shown in Figure 1, the FMR linewidth exhibits an angular dependence with a clear maximum at ∼20°, 160°, 200°, and 340° with respect to GaAs(100)[011] direction, indicating a combination of in-plane magnetic uniaxial anisotropy (UMA) and cubic magnetocrystalline anisotropy, consistent with the angular dependence of FMR resonance field, as shown in Supporting Information Figure S4b.[38] The cubic magnetocrystalline anisotropy originates from the inverse spinel structure of Fe_3O_4 crystal. However, the additional UMA is pure interfacial effect. In general, this UMA can be explained by two distinctly different mechanisms due to the Fe_3O_4/GaAs interface associated with "unidirectional chemical bonding" and "anisotropic lattice relaxation".[39−41] By fitting the thickness dependence of FMR resonance field, we found that as the thickness of Fe_3O_4 film decreases, the UMA plays an increasingly predominate role, and the cubic

DOI: 10.1021/acsami.6b09478
ACS Appl. Mater. Interfaces 2016, 8, 27353−27359

magnetocrystalline anisotropy becomes less significant, which may be related to the imperfection of the cubic symmetry due to the inevitable termination of the periodic lattice structure near the interface.[38,42,43]

It is well-known that the relaxation mechanisms of the magnetization are reflected in the FMR linewidth, which include intrinsic Gilbert-type and extrinsic non-Gilbert-type mechanisms. In general, three contributions are considered:[44]

$$\Delta H = \Delta H_{\mathrm{Gil}} + \Delta H_{\mathrm{inhom}} + \Delta H_{\mathrm{TMS}} \quad (1)$$

where the first term is intrinsic linewidth, which is proportional to Gilbert damping constant α, and it is isotropic determined by intrinsic SOC of materials. The second term of eq 1 is inhomogeneous broadening and consists of two factors. The inhomogeneous effective magnetization of the sample that results in the uneven internal field by $\Delta 4\pi M_{\mathrm{eff}}$ and the anisotropy changes over the lattice leads to the inhomogeneous magnetic orientation. With $\Delta\phi_{\mathrm{H}}$ to define the subtle difference in the azimuthal angle, the $\Delta H_{\mathrm{inhom}}$ can be expressed as

$$\Delta H_{\mathrm{inhom}} = \left|\frac{\partial H_{\mathrm{r}}}{\partial 4\pi M_{\mathrm{eff}}}\right| \Delta 4\pi M_{\mathrm{eff}} + \left|\frac{\partial H_{\mathrm{r}}}{\partial \phi_{\mathrm{H}}}\right| \Delta\phi_{\mathrm{H}} \quad (2)$$

The third term of eq 1 is caused by two-magnon scattering[45] as discussed and calculated by Mills et al.[46,47] ΔH_{TMS} is necessary to be taken into consideration when fitting the experimental data, at it is responsible for the small difference in FMR linewidths between easy and hard axes of in-plane magnetic anisotropy.

First, we consider the Fe_3O_4/GaAs films with bulklike saturation moments, that is, the films with t_{Fe} = 4 and 6 nm. Different contributions for the linewidth have been separated, as shown in Figure 2, and the fitted magnetic parameters are

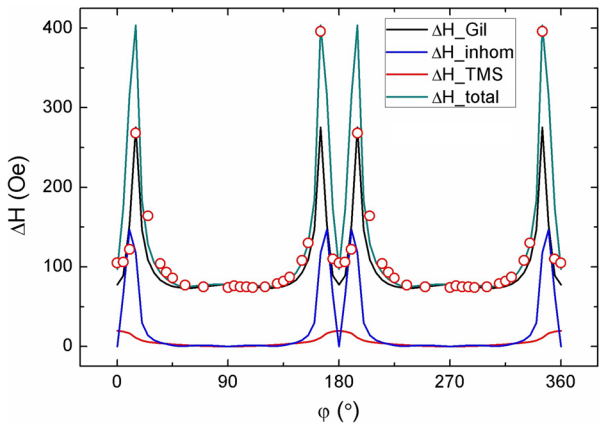

Figure 2. Angular dependence of the intrinsic linewidth, inhomogeneous, and two-magnon scattering linewidth broadening at t_{Fe} = 4 nm. The red circles represent the experimental data.

shown in Table 1, in which a great increment of inhomogeneous linewidth broadening parameter $\Delta\varphi$ with decreasing the Fe_3O_4 thickness indicates that the homogeneity of the film becomes imperfect as the thickness decreases, as the inhomogeneity most likely appears near the interface of Fe_3O_4 and GaAs. In addition, the two parameters of linewidth broadening, that is, Γ_{U} and Γ_{C}, are two-magnon scattering constants with contribution of in-plane UMA and magnetocrystalline anisotropy, and they reasonably show similar trends of thickness dependences of K_{U} and K_1. It is valuable to note that Gilbert damping constant α increases from 0.013 to 0.022 as the film thickness decreases from 6 to 4 nm. Considering α is proportional to square of the orbital-to-spin moment ratio $(m_{\mathrm{orb}}/m_{\mathrm{spin}})$,[2,48,49] the increasing α can be related to the increasing orbital moment and in turn increasing the SOC in the films,[50] which suggests that the interface effect may play an important role in the film.

Table 1. Parameters Obtained from Theoretical Fitting

t_{Fe}	α	Δm_{eff}	$\Delta\varphi$	Γ_{U}	Γ_{C}
4 nm	0.022	0	0.03	30	0
6 nm	0.013	0	0.004	0	80

The XMCD measurements were performed to quantitatively address the spin and orbital moments of the Fe_3O_4/GaAs epitaxial thin films. The resulting current output from the sample was measured in total electron yield mode as a function of the X-ray photon energy. The dichroism was obtained as the difference spectrum $I^+ - I^-$, achieved by reversing the direction of applied magnetic field at fixed polarization. Typical XAS and XMCD spectra at 300 K of the 4 and 6 nm Fe_3O_4 films are presented in Figure 3. The complex form of the XMCD spectrum arises because of an overlap of different sets of multiplet structures. The B sites Fe^{3+} and Fe^{2+} spin-up states exhibit negative peaks at Fe L_3 edge and positive peaks at the Fe L_2 edge, while the A site Fe^{3+} spin-down states behave the oppositely at the Fe L_3 and L_2 edges, respectively. The relative intensity ratio of the A and B site Fe ions in the XMCD spectrum varies with different thickness, where the intensity of B-site Fe^{2+} increases with the increasing thickness, indicating the appearance of FeO near the Fe_3O_4/GaAs interface,[37] which is attributed to the possible oxygen defects.[51,52] The orbital-to-spin moment ratio $(m_{\mathrm{orb}}/m_{\mathrm{spin}})$ was calculated by applying sum rules on the integrated XMCD of Fe L_3 and $L_{2,3}$ edges based on eq 3.[53] $m_{\mathrm{orb}}/m_{\mathrm{spin}}$ increases from 0.05 to 0.09 with decreasing thickness from 6 to 4 nm, implying the possibility of enhanced SOC, which is most likely due to the interface or surface effect.

$$\frac{m_{\mathrm{orb}}}{m_{\mathrm{spin}}} = \frac{2q}{9p - 6q} = \frac{2\int_{L2,3}(\sigma^+ - \sigma^-)\mathrm{d}E}{9\int_{L3}(\sigma^+ - \sigma^-)\mathrm{d}E - 6\int_{L2,3}(\sigma^+ - \sigma^-)\mathrm{d}E} \quad (3)$$

To gain an insight into the relation between surface/interface and the increase of orbital moment in epitaxial Fe_3O_4 thin film, we performed ab initio calculations. The SOC is a decisive factor for the orbital magnetization in solids, though generally weak for 3d transition metals,[54−56] and was included in the calculation. The optimized Fe_3O_4 unit cell (see Supporting Information Figure S3) is composed of 8 oxygen face-centered cubic (fcc) lattices (32 O anion) and 8 Fe cations occupying the tetrahedral interstices (A site, Fe_{tet}), while 16 Fe cations are located in the octahedral interstices (B site, Fe_{oct}). Fe_{tet} and Fe_{oct} ions possess antiparallel magnetic moment and thus Fe_3O_4 show ferrimagnetic properties, where the net total magnetization is mainly determined by magnetic moments of Fe_{oct} ions. The calculated lattice constant is 8.397 Å, and the local spin moments m_{spin} of the Fe_{tet} and Fe_{oct} ions are −3.76 and 3.71 μ_{B}, respectively, in good agreement with the previous experimental and calculated values.[56−58] Taking SOC into account, 0.004 and 0.010 of $m_{\mathrm{orb}}/m_{\mathrm{spin}}$ ratio of the Fe_{tet} and Fe_{oct} ions were obtained, respectively.

DOI: 10.1021/acsami.6b09478
ACS Appl. Mater. Interfaces 2016, 8, 27353−27359

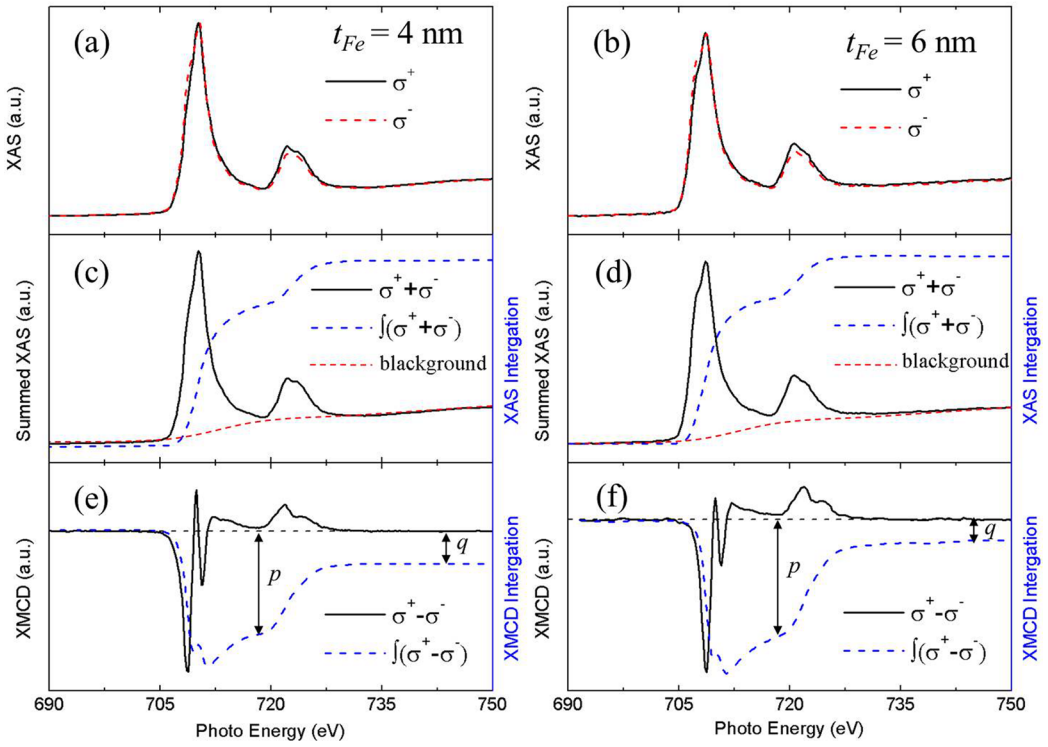

Figure 3. (a, b) XAS spectra at the Fe $L_{2,3}$ edges in Fe_3O_4 thin films with the magnetic field parallel and antiparallel to the orientation of the photon helicity. (c, d) Summed XAS spectra and its integration. The red dotted line indicates the background. (e, f) XMCD spectra and its integrations, with different thickness t_{Fe}= (a, c, e) 4 and (b, d, f) 6 nm.

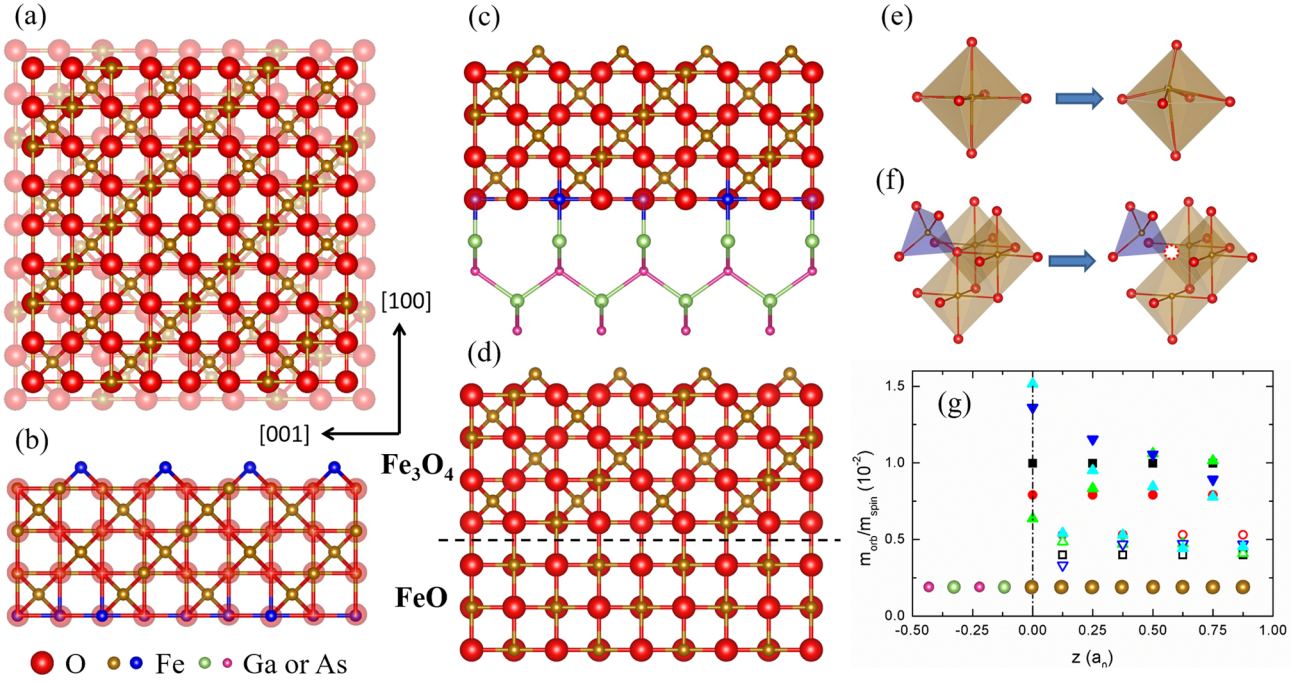

Figure 4. Schematic diagrams of calculation and the results. (a) Supercell of Fe_3O_4 with and without considering the compressive stress. (b) With the vacuum space of 15 Å on top of the supercell of Fe_3O_4, the surface Fe_{tet} (on top) and Fe_{oct} (on the bottom) ions are indicated with blue balls. (c) With the vacuum space of 15 Å on top and a supercell of GaAs on the bottom of the supercell of Fe_3O_4, the interfacial Fe_{oct} ions are illustrated with blue balls. (d) A distorted Fe_{oct} ion in the Fe_3O_4 unit cell. (e) An oxygen vacancy (dash red circle) in the Fe_3O_4 unit cell. (f) Supercell of Fe_3O_4 on FeO lattice with the dash line indicating the Fe_3O_4/FeO interface. (g) The calculated m_{orb}/m_{spin} of Fe_{tet} (hollow balls) and Fe_{oct} (solid balls) ions in the bulk (black), compression (red), surface (green), interface with Ga-terminated (dark blue), or As-terminated (light blue) GaAs model of $Fe_{24}O_{32}$ unit cell vs the distance along the (100) direction. Here the distance is normalized to the lattice constant of Fe_3O_4 (a_0 = 8.394 Å). The colored balls at the bottom indicate the position of each atomic layer.

DOI: 10.1021/acsami.6b09478
ACS Appl. Mater. Interfaces 2016, 8, 27353−27359

We first consider the stress effect induced by the mismatch of GaAs substrate. The lattice constants of Fe_3O_4 and GaAs are 8.396 and 5.654 Å. By Fe_3O_4 lattice rotating 45°, Fe_3O_4 lattice is compressed by ~5% of lattice constant on single crystal GaAs as epitaxial growth. Considering the stress only, we calculated the compressed Fe_3O_4 lattice with lattice constant of 8.00 Å, which is $\sqrt{2}$ of lattice constant of GaAs, as shown in Figure 4a. The total energy increases 2.4% for the thin films compared with the bulklike Fe_3O_4. However, the ratio m_{orb}/m_{spin} increases to 0.0057 for the Fe_{tet} ions and decreases to 0.0079 for the Fe_{oct} ions after compression, which would lead to a small decrease of net m_{orb}/m_{spin}. Therefore, the stress solely is not the origin of the increase of SOC.

We then investigate the effect of surface on m_{orb}/m_{spin} in the film. Since the film thickness decreases to the nanoscale, the magnetic properties of surface ions become significant. A vacuum space of 15 Å is set to separate the interactions between neighboring slabs of the unit cells in the (100) direction, as shown in Figure 4b, and then we have the surface Fe_{tet} ions on one side and the surface Fe_{oct} ions on the other, as indicated the blue balls in the Figure. It was found that m_{orb}/m_{spin} increases to 0.0041 for the surface Fe_{tet} ions and decreases to 0.0064 for the surface Fe_{oct} ions. The decrease of m_{orb}/m_{spin} of the surface Fe_{oct} ions originates from the increment of m_{spin}, while the m_{orb} of these ions remains unchanged. Thus, the surface effect may not be main origin of the enhanced SOC in our Fe_3O_4/GaAs system.

We also calculate the interface between Fe_3O_4 and GaAs by setting one unit cell of GaAs lattice on one side of Fe_3O_4 crystal in the (100) direction, while a vacuum space of 15 Å is set to the other, as illustrated in Figure 4c. As-or Ga-terminated surfaces are both possible for GaAs, and the interface Fe_{oct} ions are obtained, as indicated with the blue balls in the Figure. Note that, to simulate the real Fe_3O_4/GaAs interface, we also used 8.00 Å as the same lattice constant of Fe_3O_4 in this calculation as discussing the compressive stress above. From the calculation, with the interface Fe_{oct} ions bonded with Ga or As ions, m_{orb}/m_{spin} of the interface Fe_{oct} ions increases to 0.014 (Fe−Ga) or 0.015 (Fe−As), respectively, 67% of increment compared with that of the configuration with stress only. The intermixing of Fe and (or) O ions with GaAs lattice would have consequences on the magnetic properties and SOC of the samples, and three models (see Supporting Information Figure S5) of intermixing are considered. The results reveal that the total energies for all models increase enormously with the intermixing, suggesting that it is rather difficult for Fe or O ions to go into GaAs lattice. Even so, for the Fe ions in the GaAs lattice, SOC is also enhanced, which also originates from the bonding with Fe and Ga or As ions. Thus, the bonding of Fe ions and Ga or As ions at the interface would lead to the enhanced SOC in the film.

Considering that FeO might appear near the Fe_3O_4/GaAs interface, we also calculated the Fe_3O_4 lattice on FeO lattice. Bulk FeO crystallizes in rocksalt structure, and the lattice constant is 4.34 Å, leading to a small lattice mismatch between Fe_3O_4 and FeO of ~3.4%. Though all Fe^{2+} ions in FeO are located in oxygen octahedral interstice, similar to B-site Fe ions in Fe_3O_4, it is well-acknowledged that bulk FeO is a paramagnetic material at room temperature. In the calculation, we set an FeO lattice and a vacuum space of 15 Å to each side of Fe_3O_4 lattice, and we also used 8.00 Å as the same lattice constant of Fe_3O_4 as the case of Fe_3O_4/GaAs interface. The result shows that the spin and orbital moments of Fe ions in FeO near the Fe_3O_4/FeO interface increase to 0.038 and 0.030 μ_B, respectively, and the calculated m_{orb}/m_{spin} is 0.79, while those of A- and B-site Fe ions in Fe_3O_4 remain unchanged. This shows that Fe_3O_4 can induce both spin and orbital moments of Fe ions in FeO near the interface, and this might be an origin of the enhanced SOC in the films.

With the stress due to the mismatch of 5% between Fe_3O_4 and GaAs, the bottom Fe_{oct} ions are possible to distort from the center of the oxygen octahedral interstice at the interface. We calculated the distortion effect of Fe_{oct} ion, which moves only 0.1 Å (~5% of the bond length of Fe_{oct}−O) from the equilibrium position, as shown in Figure 4d, and the result shows that m_{orb}/m_{spin} of the distorted Fe_{oct} ion increases to 0.013, 30% of increment compared with bulk Fe_3O_4. The distortion of Fe_{oct} ion at the interface might also be responsible for the enhanced SOC in the film.

Strongly enhanced orbital moment was found in the interface of Fe/MgO,[59,60] Co_2FeAl/MgO,[61] Co/Pt,[62] and another system.[63,64] Some mechanisms have been reported that may be responsible for the enhanced orbital moments at the interface. (i) At the surface, interface, and the distortion configuration, the crystal-field partitioning of the electronic levels is modified, due to the reduced symmetry. Thus, the lower symmetry at the interface results in a reduced crystal-field quenching of the orbital moment and from this produces enhanced orbital moments.[65] (ii) At the surface or interface, the value of density of states (DOS) at the Fermi level E_F is larger than in the bulk, which may result in an enhanced orbital moment.[66] (iii) The induced perpendicular magnetic anisotropy at the interface is related to an increase in the orbital moment due to the hybridization between two layers.[67]

However, for the relatively thick film, that is, t_{Fe} = 8 nm, considerable FeO defects and oxygen vacancies may appear near the interface of Fe_3O_4 and GaAs due to the postgrowth oxidation method.[34,37] The Gilbert damping has also been separated from the FMR linewidth, and the damping constant was obtained. The fitting results show that the damping constant of the film increases to 0.23, 92% of increment compared with that of the film with t_{Fe} = 6 nm. As discussed above, the spin and orbital moment of Fe^{2+} ions near the interface between Fe_3O_4 and FeO defects can be induced, which might be responsible for the enhancement of SOC in relatively thick Fe_3O_4/GaAs films. Additionally, first-principle calculation provides another evidence that the oxygen vacancies in Fe_3O_4 might also be the origin of the enhanced SOC. The calculation was performed in a unit cell of Fe_3O_4 with an introducing oxygen vacancy, as illustrated in Figure 4e. The calculated m_{orb}/m_{spin} of the one Fe_{tet} and three Fe_{oct} ions neighboring the oxygen vacancy increase by a factor of 62% and 121% to 0.0060 and 0.022, respectively, and it results in a 131% increase of net m_{orb}/m_{spin}. Similar enhanced orbital moment of 3d metal due to the oxygen vacancy was found by Pavlenko et al.,[63] which involves a lowering of the local symmetry and an orbital reconstruction.

In summary, different thicknesses of ultrathin epitaxial Fe_3O_4 films were fabricated by using postoxidation method in MBE system. The FMR results show that the magnetization dynamical damping is increased by 2 times with decreasing the film thickness from 6 to 4 nm, and XMCD measurements give the direct evidence that the ratio of orbital-to-spin moment is also enhanced by nearly 2 times, which indicates that SOC may be enhanced for decreasing the film thickness, and is possibly responsible for the interface. First-principle calcu-

DOI: 10.1021/acsami.6b09478
ACS Appl. Mater. Interfaces 2016, 8, 27353−27359

lations provide the origin of enhanced SOC from different isolated surface or interface effects. It reveals that the bonding effect with Fe and Ga or As ions at the interface, the ionic distortion due to the lattice mismatch between Fe_3O_4 and GaAs, as well as FeO defects and oxygen vacancies that might appear in the relatively thick film could lead to the increase of the m_{orb}/m_{spin} of Fe ion by the factors ~30% to 131%. This work is beneficial to the design and application for ferromagnetic/semiconductor spintronic devices.

■ ASSOCIATED CONTENT

Supporting Information

The Supporting Information is available free of charge on the ACS Publications website at DOI: 10.1021/acsami.6b09478.

Schematic diagram of sample fabrication, RHEED patterns during fabrication process, calculated Fe_3O_4 lattice of a 56-atom unit cell, FMR spectra, thickness dependence of saturated magnetization moment, angular dependence of FMR resonance field, three models of intermixing layer. (PDF)

■ AUTHOR INFORMATION

Corresponding Authors

*E-mail: hzc28@seu.edu.cn. (Z.H.)
*E-mail: yazhai@seu.edu.cn. (Y.Z.)

Notes

The authors declare no competing financial interest.

■ ACKNOWLEDGMENTS

This work was supported by NSFC (Nos. 61427812, 51571062, 11504047, and 61306121) and NSF of Jiangsu Province of China (No. BK20141328).

■ REFERENCES

(1) Jungwirth, T.; Wunderlich, J.; Olejník, K. Spin Hall Effect Devices. *Nat. Mater.* **2012**, *11*, 382−390.
(2) Demidov, V. E.; Urazhdin, S.; Ulrichs, H.; Tiberkevich, V.; Slavin, A.; Baither, D.; Schmitz, G.; Demokritov, S. O. Magnetic Nano-Oscillator Driven by Pure Spin Current. *Nat. Mater.* **2012**, *11*, 1028−1031.
(3) Hasan, M. Z.; Kane, C. L. Colloquium: Topological Insulators. *Rev. Mod. Phys.* **2010**, *82*, 3045.
(4) Yu, X. Z.; Onose, Y.; Kanazawa, N.; Park, J. H.; Han, J. H.; Matsui, Y.; Tokura, Y.; et al. Real-Space Observation of a Two-Dimensional Skyrmion Crystal. *Nature* **2010**, *465*, 901−904.
(5) Liu, C. X.; Qi, X. L.; Dai, X.; Fang, Z.; Zhang, S. C. Quantum Anomalous Hall Effect in $Hg_{1-y}Mn_yTe$ Quantum Wells. *Phys. Rev. Lett.* **2008**, *101* (14), 146802.
(6) Yu, R.; Zhang, W.; Zhang, H. J.; Zhang, S. C.; Dai, X.; Fang, Z. Quantized Anomalous Hall Effect in Magnetic Topological Insulators. *Science* **2010**, *329* (5987), 61−64.
(7) Zhang, H.; Lazo, C.; Blügel, S.; Heinze, S.; Mokrousov, Y. Electrically Tunable Quantum Anomalous Hall Effect in Graphene Decorated by 5 d Transition-Metal Adatoms. *Phys. Rev. Lett.* **2012**, *108* (5), 056802.
(8) Garrity, K. F.; Vanderbilt, D. Chern Insulators from Heavy Atoms on Magnetic Substrates. *Phys. Rev. Lett.* **2013**, *110* (11), 116802.
(9) Qiao, Z.; Ren, W.; Chen, H.; Bellaiche, L.; Zhang, Z.; MacDonald, A. H.; Niu, Q. Quantum Anomalous Hall Effect in Graphene Proximity Coupled to an Antiferromagnetic Insulator. *Phys. Rev. Lett.* **2014**, *112* (11), 116404.
(10) Chang, C. Z.; Zhang, J.; Feng, X.; Shen, J.; Zhang, Z.; Guo, M.; Xue, Q. K.; et al. Experimental Observation of the Quantum Anomalous Hall Effect in a Magnetic Topological Insulator. *Science* **2013**, *340*, 167−170.
(11) Chen, Y. L.; Chu, J. H.; Analytis, J. G.; Liu, Z. K.; Igarashi, K.; Kuo, H. H.; Shen, Z. X.; et al. Massive Dirac Fermion on the Surface of a Magnetically Doped Topological Insulator. *Science* **2010**, *329*, 659−662.
(12) Zhang, J.; Chang, C. Z.; Tang, P.; Zhang, Z.; Feng, X.; Li, K.; Wang, Y.; et al. Topology-Driven Magnetic Quantum Phase Transition in Topological Insulators. *Science* **2013**, *339*, 1582−1586.
(13) Kou, X.; Guo, S. T.; Fan, Y.; Pan, L.; Lang, M.; Jiang, Y.; Wang, K. L.; et al. Scale-Invariant Quantum Anomalous Hall Effect in Magnetic Topological Insulators beyond the Two-Dimensional Limit. *Phys. Rev. Lett.* **2014**, *113*, 137201.
(14) Hu, J.; Zhu, Z.; Wu, R. Chern Half Metals: A New Class of Topological Materials to Realize the Quantum Anomalous Hall Effect. *Nano Lett.* **2015**, *15*, 2074−2078.
(15) Lin, X.; Ni, J. Half-Metallicity in Graphene Nanoribbons with Topological Line Defects. *Phys. Rev. B: Condens. Matter Mater. Phys.* **2011**, *84* (7), 075461.
(16) Xiao, D.; Yao, Y.; Feng, W.; Wen, J.; Zhu, W.; Chen, X. Q.; Zhang, Z.; et al. Half-Heusler Compounds as a New Class of Three-Dimensional Topological Insulators. *Phys. Rev. Lett.* **2010**, *105* (9), 096404.
(17) Dedkov, Y. S.; Rüdiger, U.; Güntherodt, G. Evidence for the Half-Metallic Ferromagnetic State of Fe_3O_4 by Spin-Resolved Photoelectron Spectroscopy. *Phys. Rev. B: Condens. Matter Mater. Phys.* **2002**, *65*, 064417.
(18) Antonov, V. N.; Harmon, B. N.; Yaresko, A. N. Electronic Structure and X-Ray Magnetic Circular Dichroism in Fe_3O_4 and Mn-, Co−, or Ni-Substituted Fe_3O_4. *Phys. Rev. B: Condens. Matter Mater. Phys.* **2003**, *67*, 024417.
(19) Fonin, M.; Pentcheva, R.; Dedkov, Y. S.; Sperlich, M.; Vyalikh, D. V.; Scheffler, M.; Güntherodt, G.; et al. Surface Electronic Structure of the Fe_3O_4(100): Evidence of a Half-Metal to Metal Transition. *Phys. Rev. B: Condens. Matter Mater. Phys.* **2005**, *72* (10), 104436.
(20) Wang, W. G.; Li, M.; Hageman, S.; Chien, C. L. Electric-Field-Assisted Switching in Magnetic Tunnel Junctions. *Nat. Mater.* **2011**, *11* (1), 64−68.
(21) Liu, W. Q.; Xu, Y. B.; Wong, P. K. J.; Maltby, N. J.; Li, S. P.; Wang, X. F.; Zhang, R.; et al. Spin and Orbital Moments of Nanoscale Fe_3O_4 Epitaxial Thin Film on MgO/GaAs(100). *Appl. Phys. Lett.* **2014**, *104*, 142407.
(22) Liu, W. Q.; Song, M. Y.; Maltby, N. J.; Li, S. P.; Lin, J. G.; Samant, M. G.; Parkin, S. S. P.; Bencok, P.; Steadman, P.; Dobrynin, A.; Xu, Y. B.; Zhang, R. X-ray Magnetic Circular Dichroism Study of Epitaxial Magnetite Ultrathin Film on MgO (100). *J. Appl. Phys.* **2015**, *117*, 17E121.
(23) Kim, K. W.; Lee, H. W.; Lee, K. J.; Stiles, M. D. Chirality from Interfacial Spin-Orbit Coupling Effects in Magnetic Bilayers. *Phys. Rev. Lett.* **2013**, *111* (21), 216601.
(24) Ryu, K. S.; Thomas, L.; Yang, S. H.; Parkin, S. Chiral Spin Torque at Magnetic Domain Walls. *Nat. Nanotechnol.* **2013**, *8* (7), 527−533.
(25) Bode, M.; Heide, M.; Von Bergmann, K.; Ferriani, P.; Heinze, S.; Bihlmayer, G.; Wiesendanger, R.; et al. Chiral Magnetic Order at Surfaces Driven by Inversion Asymmetry. *Nature* **2007**, *447* (7141), 190−193.
(26) Liu, L.; Pai, C. F.; Li, Y.; Tseng, H. W.; Ralph, D. C.; Buhrman, R. A. Spin-Torque Wwitching with the Giant Spin Hall Effect of Tantalum. *Science* **2012**, *336* (6081), 555−558.
(27) Kim, K. W.; Lee, H. W.; Lee, K. J.; Stiles, M. D. Chirality from Interfacial Spin-Orbit Coupling Effects in Magnetic Bilayers. *Phys. Rev. Lett.* **2013**, *111* (21), 216601.
(28) Pesin, D.; Balents, L. Mott Physics and Band Topology in Materials with Strong Spin−Orbit Interaction. *Nat. Phys.* **2010**, *6* (5), 376−381.
(29) Lu, Y. X.; Claydon, J. S.; Xu, Y. B.; Thompson, S. M.; Wilson, K.; Van der Laan, G. Epitaxial Growth and Magnetic Properties of

Half-Metallic Fe_3O_4 on GaAs (100). *Phys. Rev. B: Condens. Matter Mater. Phys.* **2004**, *70*, 233304.
(30) Blöchl, P. E. Projector Augmented-Wave Method. *Phys. Rev. B: Condens. Matter Mater. Phys.* **1994**, *50* (24), 17953.
(31) Perdew, J. P.; Burke, K.; Ernzerhof, M. Generalized Gradient Approximation Made Simple. *Phys. Rev. Lett.* **1996**, *77* (18), 3865.
(32) Kresse, G.; Hafner, J. *Ab Initio* Molecular Dynamics for Liquid Metals. *Phys. Rev. B: Condens. Matter Mater. Phys.* **1993**, *47* (1), 558.
(33) Monkhorst, H. J.; Pack, J. D. Special Points for Brillouin-Zone Integrations. *Phys. Rev. B* **1976**, *13* (12), 5188.
(34) Huang, Z.; Chen, Q.; Zhai, Y.; Wang, J.; Xu, Y.; Wang, B. Oxygen Vacancy Induced Magnetization Witching in Fe_3O_4 Epitaxial Ultrathin Films on GaAs (100). *Appl. Phys. Lett.* **2015**, *106*, 182401.
(35) Lindner, J.; Meckenstock, R.; Farle, M. In *Characterization of Materials,* 2nd ed.; Kaufmann, E. N., Ed.; John Wiley & Sons: New York, 2012, pp 1−20.
(36) Farle, M.; Silva, T.; Woltersdorf, G. In *Magnetic Nanostructures,* 1st ed.; Springer: New York, 2013; pp 37−83.
(37) Lu, Y. X.; Claydon, J. S.; Ahmad, E.; Xu, Y. B.; Thompson, S. M.; Wilson, K.; Van der Laan, G. XPS and XMCD Study of Fe_3O_4/GaAs Interface. *IEEE Trans. Magn.* **2005**, *41* (10), 2808−2810.
(38) Zhai, Y.; Huang, Z. C.; Fu, Y.; Ni, C.; Lu, Y. X.; Xu, Y. B.; Wu, J.; Zhai, H. R. Anisotropy of Ultrathin Epitaxial Fe_3O_4 Films on GaAs(100). *J. Appl. Phys.* **2007**, *101*, 09D126.
(39) Thomas, O.; Shen, Q.; Schieffer, P.; Tournerie, N.; Lépine, B. Interplay between Anisotropic Strain Relaxation and Uniaxial Interface Magnetic Anisotropy in Epitaxial Fe Films on (001) GaAs. *Phys. Rev. Lett.* **2003**, *90* (1), 017205.
(40) Prinz, G. A. In *Ultrathin Magnetic Structures;* Heinrich, B., Bland, J. A. C., Eds.; Springer-Verlag: Berlin, Germany, 1994; Vol. *II*, pp 1−44.
(41) Xu, Y. B.; Freeland, D. J.; Tselepi, M.; Bland, J. A. C. Anisotropic Lattice Relaxation and Uniaxial Magnetic Anisotropy in Fe/InAs(100)−4 × 2. *Phys. Rev. B: Condens. Matter Mater. Phys.* **2000**, *62* (2), 1167.
(42) Zhai, Y.; Sun, L.; Huang, Z. C.; Lu, Y. X.; Li, G. D.; Li, Q.; Xu, Y. B.; Wu, J.; Zhai, H. R. Thickness Dependence of the Molecular Magnetic Moment of Single Crystal Fe_3O_4 Films on GaAs (100). *J. Appl. Phys.* **2010**, *107* (9), 09B110.
(43) Zhang, W.; Zhang, J. Z.; Wong, P. K. J.; Huang, Z. C.; Sun, L.; Liao, J. L.; Zhai, Y.; Xu, Y. B.; van der Laan, G. In-plane Uniaxial Magnetic Anisotropy in Epitaxial Fe_3O_4-Based Hybrid Structures on GaAs(100). *Phys. Rev. B: Condens. Matter Mater. Phys.* **2011**, *84*, 104451.
(44) Luo, C.; Feng, Z.; Fu, Y.; Zhang, W.; Wong, P. K. J.; Kou, Z. X.; Zhai, H. R.; et al. Enhancement of Magnetization Damping Coefficient of Permalloy Thin Films with Dilute Nd Dopants. *Phys. Rev. B: Condens. Matter Mater. Phys.* **2014**, *89* (18), 184412.
(45) Sparks, M. *Ferromagnetic Relaxation Theory* McGraw-Hill: New York, 1966.
(46) Arias, R.; Mills, D. L. Extrinsic Contributions to the Ferromagnetic Resonance Response of Ultrathin Films. *Phys. Rev. B: Condens. Matter Mater. Phys.* **1999**, *60* (10), 7395.
(47) Landeros, P.; Arias, R. E.; Mills, D. L. Two Magnon Scattering in Ultrathin Ferromagnets: The Case Where the Magnetization is Out of Plane. *Phys. Rev. B: Condens. Matter Mater. Phys.* **2008**, *77* (21), 214405.
(48) Kittel, C. On the Gyromagnetic Ratio and Spectroscopic Splitting Factor of Ferromagnetic Substances. *Phys. Rev.* **1949**, *76* (6), 743.
(49) Farle, M. Ferromagnetic Resonance of Ultrathin Metallic Layers. *Rep. Prog. Phys.* **1998**, *61* (7), 755.
(50) Zhang, W.; Zhang, D.; Wong, P. K. J.; Yuan, H. L.; Jiang, S.; van der Laan, G.; Zhai, Y.; Lu, Z. H. Selective Tuning of Gilbert Damping in Spin-Valve Trilayer by Insertion of Rare-Earth Nanolayers. *ACS Appl. Mater. Interfaces* **2015**, *7*, 17070−17075.
(51) Paul, M.; Müller, A.; Ruff, A.; Schmid, B.; Berner, G.; Mertin, M.; Sing, M.; Claessen, R. Probing the Interface of Fe_3O_4/GaAs Thin Films by Hard X-Ray Photoelectron Spectroscopy. *Phys. Rev. B: Condens. Matter Mater. Phys.* **2009**, *79* (23), 233101.
(52) Morrall, P.; Schedin, F.; Case, G. S.; Thomas, M. F.; Dudzik, E.; Van der Laan, G.; Thornton, G. Stoichiometry of $Fe_{3-\delta}O_4$ (111) Ultrathin Films on Pt (111). *Phys. Rev. B: Condens. Matter Mater. Phys.* **2003**, *67* (21), 214408.
(53) Thole, B. T.; Carra, P.; Sette, F.; van der Laan, G. X-ray Circular Dichroism as a Probe of Orbital Magnetization. *Phys. Rev. Lett.* **1992**, *68*, 1943.
(54) Tokura, Y.; Nagaosa, N. Orbital Physics in Transition-Metal Oxides. *Science* **2000**, *288* (5465), 462−468.
(55) Tung, J. C.; Guo, G. Y. Systematic *Ab Initio* Study of the Magnetic and Electronic Properties of All 3d Transition Metal Linear and Zigzag Nanowires. *Phys. Rev. B: Condens. Matter Mater. Phys.* **2007**, *76* (9), 094413.
(56) Szotek, Z.; Temmerman, W. M.; Svane, A.; Petit, L.; Stocks, G. M.; Winter, H. *Ab Initio* Study of Charge Order in Fe_3O_4. *Phys. Rev. B: Condens. Matter Mater. Phys.* **2003**, *68* (5), 054415.
(57) Cheng, C. Structure and Magnetic Properties of the Fe_3O_4(001) Surface: *Ab initio* Studies. *Phys. Rev. B: Condens. Matter Mater. Phys.* **2005**, *71* (5), 052401.
(58) Ziese, M.; Esquinazi, P. D.; Pantel, D.; Alexe, M.; Nemes, N. M.; Garcia-Hernández, M. Magnetite (Fe_3O_4): a New Variant of Relaxor Multiferroic? *J. Phys.: Condens. Matter* **2012**, *24* (8), 086007.
(59) Yang, H. X.; Chshiev, M.; Dieny, B.; Lee, J. H.; Manchon, A.; Shin, K. H. First-Principles Investigation of the Very Large Perpendicular Magnetic Anisotropy at Fe/MgO and Co/MgO Interfaces. *Phys. Rev. B: Condens. Matter Mater. Phys.* **2011**, *84* (5), 054401.
(60) Jal, E.; Kortright, J. B.; Chase, T.; Liu, T.; Gray, A. X.; Shafer, P.; Dürr, H. A.; et al. Interface Fe Magnetic Moment Enhancement in MgO/Fe/MgO Trilayers. *Appl. Phys. Lett.* **2015**, *107* (9), 092404.
(61) Okabayashi, J.; Sukegawa, H.; Wen, Z.; Inomata, K.; Mitani, S. Large Anisotropic Fe Orbital Moments in Perpendicularly Magnetized Co_2FeAl Heusler Alloy Thin Films Revealed by Angular-Dependent X-Ray Magnetic Circular Dichroism. *Appl. Phys. Lett.* **2013**, *103* (10), 102402.
(62) Haney, P. M.; Lee, H. W.; Lee, K. J.; Manchon, A.; Stiles, M. D. Current-Induced Torques and Interfacial Spin-Orbit Coupling. *Phys. Rev. B: Condens. Matter Mater. Phys.* **2013**, *88* (21), 214417.
(63) Yildiz, F.; Luo, F.; Tieg, C.; Abrudan, R. M.; Fu, X. L.; Winkelmann, A.; Kirschner, J.; et al. Strongly Enhanced Orbital Moment by Reduced Lattice Symmetry and Varying Composition of $Fe_{1-x}Co_x$ Alloy Films. *Phys. Rev. Lett.* **2008**, *100* (3), 037205.
(64) Bruno, F. Y.; Garcia-Barriocanal, J.; Varela, M.; Nemes, N. M.; Thakur, P.; Cezar, J. C.; Santamaria, J.; et al. Electronic and Magnetic Reconstructions in $La_{0.7}Sr_{0.3}MnO_3/SrTiO_3$ Heterostructures: A Case of Enhanced Interlayer Coupling Controlled by the Interface. *Phys. Rev. Lett.* **2011**, *106* (14), 147205.
(65) Tischer, M.; Hjortstam, O.; Arvanitis, D.; Hunter Dunn, J.; May, F.; Baberschke, K.; Eriksson, O.; et al. Enhancement of Orbital Magnetism at Surfaces: Co on Cu (100). *Phys. Rev. Lett.* **1995**, *75* (8), 1602.
(66) Eriksson, O.; Nordström, L.; Pohl, A.; Severin, L.; Boring, A. M.; Johansson, B. Spin and Orbital Magnetism in 3d Systems. *Phys. Rev. B: Condens. Matter Mater. Phys.* **1990**, *41* (17), 11807.
(67) Pavlenko, N.; Kopp, T.; Tsymbal, E. Y.; Mannhart, J.; Sawatzky, G. A. Oxygen Vacancies at Titanate Interfaces: Two-Dimensional Magnetism and Orbital Reconstruction. *Phys. Rev. B: Condens. Matter Mater. Phys.* **2012**, *86* (6), 064431.

DOI: 10.1021/acsami.6b09478
ACS Appl. Mater. Interfaces 2016, 8, 27353−27359